Supplementary Information
Mechanisms of soil organic carbon and nitrogen stabilization in mineral associated organic matter – Insights from modelling in phase space

Stefano Manzoni[1], Francesca Cotrufo[2]

[1]Department of Physical Geography and Bolin Centre for Climate Research, Stockholm University, SE-106 91 Stockholm, Sweden
[2]Department of Soil and Crop Sciences, Colorado State University, Fort Collins, CO, USA

Correspondence to: Stefano Manzoni (stefano.manzoni@natgeo.su.se)

S1. Generalized model including dissolved organic matter dynamics

C and N are transferred between POM and MAOM compartments partly via dissolved organic matter (DOM), which is only considered implicitly in the model presented in the main text (Fig. 1). In this appendix, we present a more general model including a DOM compartment, and show which simplifications lead to the model used in the main text. To construct this more general model, we assume that a fraction of the depolymerized products from POM and MAOM are used locally by the respective microbial communities (fractions $1-l_P$ and $1-l_M$, respectively) and a fraction is transferred to a 'shared' DOM compartment (fractions l_P and l_M, respectively). DOM is then taken up by both communities according to the rates U_P and U_M (Fig. S1).

The C mass balance equations for the substrate (second subscript *S*), microbial biomass (second subscript *B*) in the POM (first subscript *P*) and MAOM (first subscript *M*), as well as for the DOM (subscript *D*) can be written as,

$$\frac{dC_{PS}}{dt} = -\underbrace{(1-l_P)D_P}_{uptake} - \underbrace{l_P D_P}_{POM\to DOM} + \underbrace{(1-m)M_P}_{recycled\ mortality}, \quad (1)$$

$$\frac{dC_{PB}}{dt} = \underbrace{e_P U_P}_{growth\ on\ DOM} + \underbrace{(1-l_P)e_P D_P}_{growth\ on\ POM} - \underbrace{M_P}_{mortality}, \quad (2)$$

$$\frac{dC_{MS}}{dt} = -\underbrace{(1-l_M)D_M}_{uptake} - \underbrace{l_M D_M}_{MAOM\to DOM} + \underbrace{mM_P}_{in\ vivo} + \underbrace{M_M}_{mortality}, \quad (3)$$

$$\frac{dC_{MB}}{dt} = \underbrace{e_M U_M}_{growth\ on\ DOM} + \underbrace{(1-l_M)e_M D_M}_{growth\ on\ MAOM} - \underbrace{M_M}_{mortality}, \quad (4)$$

$$\frac{dC_D}{dt} = \underbrace{l_P D_P}_{POM\to DOM} + \underbrace{l_M D_M}_{MAOM\to DOM} - \underbrace{(U_P+U_M)}_{uptake}. \quad (5)$$

The rate of uptake of DOM by the POM microbes is probably smaller than the uptake by MAOM microbes, as the former primarily feed on POM substrates (i.e., $U_P \approx 0$). Moreover, we can assume that the DOM compartment is in quasi-

equilibrium (i.e., $dC_D/dt \approx 0$) because it is a small C compartment with relatively fast turnover rates. Mathematically, this means that $U_M \approx l_P D_P + l_M D_M$, which allows simplifying Eq. (1)-(5) and obtain the model described in the main text (after re-naming $l = l_P$).

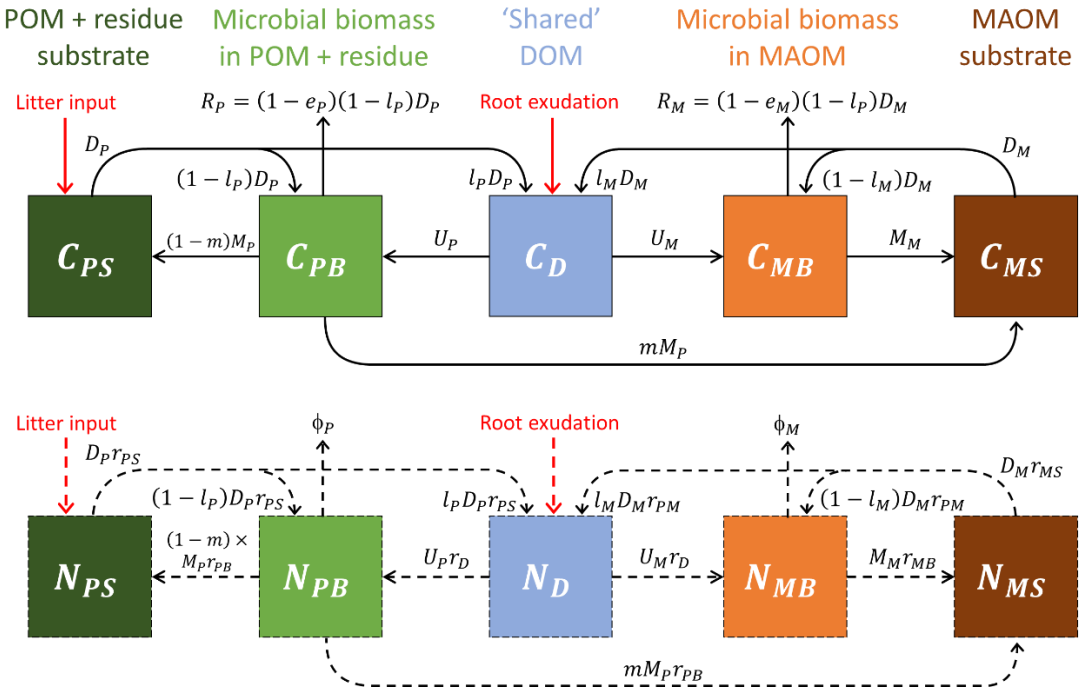

Figure S1. Schematic of the generalized model including a dissolved organic matter (DOM) compartment. Solid and dashed arrows or compartment edges indicate respectively C and N flows or compartments. Plant input rates to POM (litter) and DOM (root exudates) are shown as red arrows, but are not included in the model equations because a single cohort of residues is tracked during decomposition and stabilization.

S2. General solutions for partly soluble residues ($b < 1$)

The following equations are the general solutions of Eq. (10) (for $c_M(c_P)$) and (24) (for $n_P(c_P)$) in the main text when the added residues are partly soluble ($b < 1$),

$$c_M = \frac{c_P\left(l+\frac{am}{1-m}\right)+\left(\frac{c_P}{b}\right)^{\frac{\kappa(1-e_M)}{1-a}}\left\{(1-b)[\kappa(1-e_M)-1]-bl+a\left(1-\frac{b}{1-m}\right)\right\}}{\kappa(1-e_M)+a-1}, \quad (6)$$

$$n_P = c_P\frac{r_B}{r_0} + \left(1-\frac{r_B}{r_0}\right)b\left(\frac{c_P}{b}\right)^{\frac{1}{1-a}}. \quad (7)$$

The full analytical solution of Eq. (26) for $n_M(c_P)$ is rather cumbersome and less mathematically insightful, so we do not report it here. These equations can be simplified as done in the main text by substituting $a = e_P(1-l)(1-m)$, simplifying where possible the factor $1-m$, taking the limit for $m \to 1$ (as motivated in Section 3.2), and further assuming that all microbes have the same CUE (e). These simplifications lead to the more compact solutions,

$$c_M = c_P\frac{l(1-e)+e}{\kappa(1-e)-1} + \left(\frac{c_P}{b}\right)^{\kappa(1-e_M)}\left\{1-b\left[1-\frac{l(1-e)+e}{\kappa(1-e)-1}\right]\right\}, \quad (8)$$

$$n_P = c_P, \quad (9)$$

$$n_M = c_P\left[l-\frac{(\kappa+l-1)e}{1-\kappa(1-e)}\frac{r_B}{r_0}\right]\frac{1}{\kappa-1} + \left(\frac{c_P}{b}\right)^{\kappa}\left[1-\frac{b(\kappa+l-1)}{\kappa-1}\right]\left(1-\frac{r_B}{r_0}\right) + \left(\frac{c_P}{b}\right)^{\kappa(1-e)}\left[1+\frac{b(\kappa+l-1)(1-e)}{1-\kappa(1-e)}\right]\frac{r_B}{r_0}, \quad (10)$$

with boundary conditions $c_M(b) = 1-b$, $n_P(b) = b$, and $n_M(b) = 1-b$.

Fig. S2 illustrate the effect of residue solubility, mathematically represented by the parameter b. Compared to insoluble residues ($b = 1$), residues whose fraction $1-b$ is immediately stabilized in MAOM have initial conditions at lower c_P and n_P, but correspondingly higher c_M and n_M levels (red circles in Fig. S2). Despite these different initial states, the trajectories of c_M, n_P, and n_M in phase space generally converge to those of residues with $b = 1$ as decomposition progresses. However, lower values of microbial CUE (low e) and when MAOM is decomposed much slower than POM + residues (low κ) cause the trajectories of c_M to remain separated for a longer period compared to the trajectories of n_P, and n_M (top panels in Fig. S2).

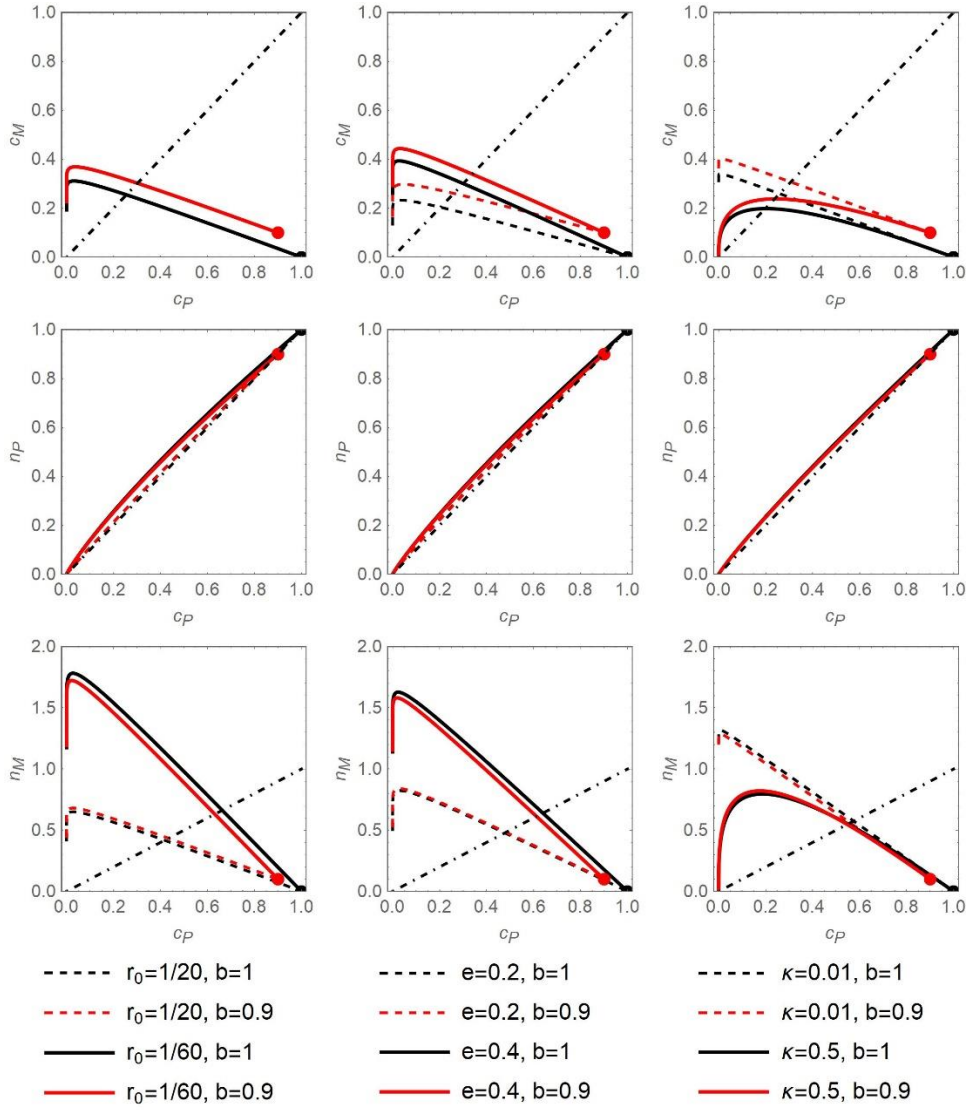

Figure S2. Fraction of added C in MAOM, c_M (top row), fraction of added N in POM + residues, n_P (center row), and fraction of added N in MAOM, n_M (bottom row), as a function of the fraction of added C in POM + residues, c_P, at different levels of residue solubility (colors) and when varying the values of model parameters: residue N:C ratio, r_0 (left column), microbial carbon use efficiency, e (center column), and ratio between the decay constants of MAOM and POM + residue decomposition, κ (right column). Two solubility levels are considered: insoluble residues ($b = 1$; black), and partly soluble residues resulting in rapid stabilization of a fraction of residue ($b = 0.9$; red). In all panels, residue decomposition progresses from right to left along the curves, as c_P decreases; initial conditions are indicated by circles; the dot-dashed black lines indicate 1:1 lines, which represent equality between the fractions of added C or N shown on the y-axes and c_P shown on the x-axes. Baseline parameters are: $l = 0.1$, $m = 0.9$, $r_0 = 1/40$, $e = 0.3$, $\kappa = 0.05$.

S3. Comparison of models assuming insoluble ($b = 1$) or partly soluble residues ($b < 1$)

To assess if model fitting improves when considering partial stabilization of soluble residues, we selected five datasets with sufficient resolution at the beginning of decomposition (when the effect of the initial condition is most relevant) and fitted two model versions: one with $b = 1$ and one with $b < 1$. These five datasets (from four studies) tracked the fate of C from various types of grass and herb residues (Lavallee et al., 2018; Mitchell et al., 2018; Leichty et al., 2021; Nunez et al., 2022). Assuming that ~10% of residue C is water soluble, and that approximately half of that can be readily stabilized, we obtain an estimate for $b = 0.95$ (i.e., initial MAOM fraction is 0.05). For reference, ~20% of C in leachate can be stabilized as MAOM in one week (Even and Cotrufo, 2024), suggesting that the 50% figure. we considered is at the high end of a reasonable range. In principle, b could be regarded as a fitting parameter as well, but most datasets lacked data points in the initial phases of decomposition (i.e., $c_P > 0.8$) so that b cannot be properly constrained. We could also estimate b from measured soluble C fractions for each residue type across the database, but these estimates would still be uncertain as we do not know how much of the soluble C is used locally by microorganisms in the POM + residue compartment and how much can be transported away and stabilized as MAOM. Therefore, we limit this model comparison to the two end-member cases of $b = 1$ and $b = 0.95$.

The comparison between these two model versions is shown in Fig. S3. For some residue types, the measured fraction of added C in MAOM was much lower than 0.05, indicating that in those datasets very little soluble C was stabilized at the beginning of decomposition. In other datasets data seemed instead consistent with an initial fraction of added C in MAOM of about 0.05. Overall, the model assuming $b = 1$ performed better than or comparably to the model assuming $b = 0.95$ in five out of six datasets (lower or similar root mean square error). Therefore, considering the uncertainties around the value of b and lack of high frequency data to constrain the other model parameters, we can conclude that it is reasonable to assume $b = 1$ across the database.

The parameters estimated with the two models were numerically different but highly correlated between models (Pearson correlation coefficients $\gtrsim 0.9$; Fig. S4). Specifically, the values of microbial CUE were slightly lower when assuming $b < 1$, while the fractions of depolymerized C stabilized as MAOM were much lower. This is expected because the two model versions are constrained to fit the same MAOM data. As a consequence, when more C is initially stabilized as MAOM ($b = 0.95$), less C will be stabilized at later stages (lower l). The high correlation between parameter values estimated with the two models suggests that conclusions on the significance and direction of the effects of soil and environmental drivers on e and l (Section 3.4 in the main text) are likely to be robust to variations in residue solubility.

More detailed studies of the fate of soluble C within days after the start of decomposition, or studies reporting MAOM at high frequency during the first days or weeks could provide constraints on the value of b. The equations reported in this Supplementary Materials are ready to be tested with such data.

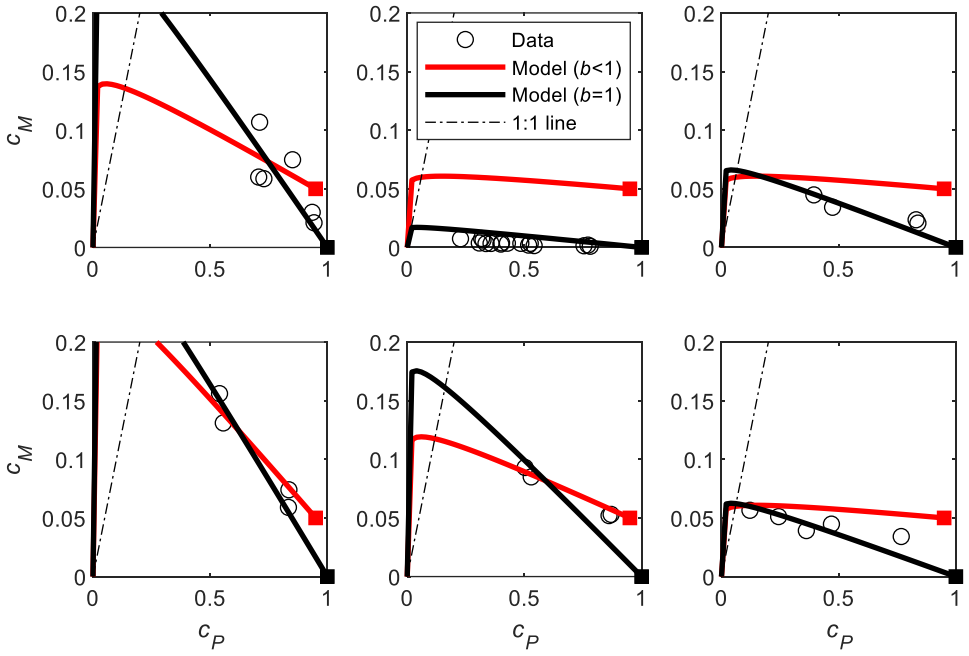

Figure S3. Fraction of added C in MAOM, c_M, as a function of the fraction of added C in POM + residues, c_P, at different levels of residue solubility (black: $b = 1$; red: $b = 0.95$) in five datasets where measurements during the early phase of decomposition ($c_P > 0.75$) were available (Cotrufo et al., 2015; Lavallee et al., 2018; Mitchell et al., 2018; Leichty et al., 2021; Nunez et al., 2022). Curves are least square model fitting to the data using Equation (8) with $\kappa = 0.05$ and e and l as fitting parameters (shown in Fig. S4). In all panels, residue decomposition progresses from right to left along the curves, as c_P decreases; initial conditions are indicated by filled squares; the dot-dashed black lines indicate 1:1 lines.

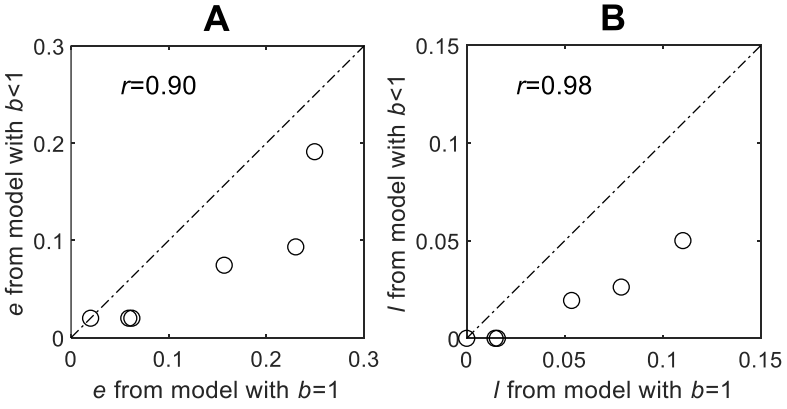

Figure S4. Comparisons between parameters estimated when assuming that the added residues were insoluble ($b = 1$, black curves in Fig. S3) or partly soluble ($b = 0.95$, red curves in Fig. S3): A) comparison of microbial C use efficiencies (e) and B) comparison of fractions of depolymerized C stabilized in MAOM (l). The dot-dashed black lines indicate 1:1 lines; r: Pearson correlation coefficients.

S4. Data

Table S1. Sources and types of data.

Data source	# treatments or sites	# residue types	residue source	# time points	C compartments				N compartments			
					residues	POM	residues + POM	MAOM	residues	POM	residues + POM	MAOM
Almeida et al. (2021)	1	4	P	1			×	×				
Antonio Telles Rodrigues et al. (2022)	5	1	P	1	×	×	×	×				
Buckeridge et al. (2022; 2021)	4	3	P, M	4			×	×			×	×
Canisares et al. (2023)	2	3	P	1	×	×	×	×				
Cheng et al. (2023)	1	4	P	3			×	×				
Cotrufo et al. (2015)	1	1	P	5	×	×	×	×	×			
Cotrufo et al. (2022)	2	5	P, O	1	×	×	×	×	×	×	×	×
Craig et al. (2022, 2021)	1	16	P	2	×		×	×				
Dai et al. (2022)	3	1	P	1			×	×				
Duan et al. (2023)	3	1	P	3		×		×				
Even and Cotrufo (2024)	4	1	P, O	2	×	×	×	×				
Fang et al. (2019)	12	1	P	2			×	×				
Ferreira et al. (2021), Oliveira et al. (2021)	2	2	P	2	×	×	×	×				
Fulton-Smith and Cotrufo (2019)	1	2	P	3	×	×	×	×	×	×	×	×
Haddix et al. (2020)	10	1	P	2			×	×				
Pries et al. (2017)	1	2	P	5	×	×	×	×	×	×	×	×
Pries et al. (2018)	3	1	P	3	×	×	×	×				
Huys et al. (2022a, b)	1	24	P	4	×	×	×	×				
Kölbl et al. (2007, 2006)	2	1	P	4		×		×		×		×
Kou et al. (2023b, a)	3	1	P	4	×	×	×	×				
Lavallee et al. (2018)	2	2	P	2			×	×			×	×
Leichty et al. (2021)	3	1	P	2	×	×	×	×				
Lian et al. (2016)	1	3	P	1	×	×	×	×				
Liebmann et al. (2020)	1	1	P	2	×	×	×	×				

Lyu et al. (2023)	1	2	P	2	×	×	×	×				
Magid et al. (2002)	1	1	P	3			×	×				
Mitchell et al. (2018)	4	1	P	4	×	×	×	×	×	×	×	×
Neupane et al. (2023)	6	1	P	3	×	×	×	×				
Nunez et al. (2022)	2	1	P	2	×	×	×	×	×	×	×	×
Nyamasoka-Magonziwa et al. (2022)	2	3	P, O	1		×		×				
Poeplau et al. (2023)	2	4	P	3			×	×				
Ridgeway et al. (2022)	2	4	P	1			×	×			×	×
Ridgeway et al. (2023b, a)	9	1	P	1			×	×			×	×
Schiedung et al. (2023)	11	2	P, O	1			×	×				
Sokol et al. (2019)	1	3	P	1		×		×				
Su et al. 2020	1	1	P	5		×		×				
Throckmorton et al. (2015)	2	1	M	5			×	×				
Wang et al. (2017)	1	4	P	4		×		×				
Xu et al. (2022)	4	2	P	1	×	×	×	×				

P: plant (leaves, shoots, roots, woody material), M: microbial necromass, O: other residues (e.g., manure, leachates)

×: the data source includes some data points in the marked category, but not always in all treatment/site/residue type combinations

References

Almeida, L., Souza, I., Hurtarte, L., Teixeira, P., Inagaki, T., Silva, I., and Mueller, C.: Forest litter constraints on the pathways controlling soil organic matter formation, Soil Biology & Biochemistry, 163, https://doi.org/10.1016/j.soilbio.2021.108447, 2021.

Antonio Telles Rodrigues, L., Giacomini, S. J., Dieckow, J., Cherubin, M. R., Sangiovo Ottonelli, A., and Bayer, C.: Carbon saturation deficit and litter quality drive the stabilization of litter-derived C in mineral-associated organic matter in long-term no-till soil, CATENA, 219, 106590, https://doi.org/10.1016/j.catena.2022.106590, 2022.

Buckeridge, K., Mason, K., Ostle, N., McNamara, N., Grant, H., and Whitaker, J.: Microbial necromass carbon and nitrogen persistence are decoupled in agricultural grassland soils, Communications Earth & Environment, 3, https://doi.org/10.1038/s43247-022-00439-0, 2022.

Buckeridge, K. M.: kmbuckeridge/UGrass_NecromassCNstabilization: Necromass CN stabilization (v1.0), https://doi.org/10.5281/zenodo.5036539, 2021.

Canisares, L., Banet, T., Rinehart, B., McNear, D., and Poffenbarger, H.: Litter quality and living roots affected the formation of new mineral-associated organic carbon but did not affect total mineral-associated organic carbon in a short-term incubation, Geoderma, 430, https://doi.org/10.1016/j.geoderma.2022.116302, 2023.

Cheng, X., Xing, W., and Liu, J.: Litter chemical traits, microbial and soil stoichiometry regulate organic carbon accrual of particulate and mineral-associated organic matter, Biology and Fertility of Soils, https://doi.org/10.1007/s00374-023-01746-0, 2023.

Cotrufo, M., Soong, J., Horton, A., Campbell, E., Haddix, M., Wall, D., and Parton, A.: Formation of soil organic matter via biochemical and physical pathways of litter mass loss, Nature Geoscience, 8, 776-+, https://doi.org/10.1038/NGEO2520, 2015.

Cotrufo, M., Haddix, M., Kroeger, M., and Stewart, C.: The role of plant input physical-chemical properties, and microbial and soil chemical diversity on the formation of particulate and mineral-associated organic matter, Soil Biology & Biochemistry, 168, https://doi.org/10.1016/j.soilbio.2022.108648, 2022.

Craig, M., Geyer, K., Beidler, K., Brzostek, E., Frey, S., Grandy, A., Liang, C., and Phillips, R.: Fast-decaying plant litter enhances soil carbon in temperate forests but not through microbial physiological traits, Nature Communications, 13, https://doi.org/10.1038/s41467-022-28715-9, 2022.

Craig, M. E., Brzostek, E. R., Geyer, K. M., Liang, C., and Phillips, R. P.: Data for "Fast-decaying plant litter enhances soil carbon in temperate forests, but not through microbial physiological traits," https://doi.org/10.15485/1835182, 2021.

Dai, S., He, P., Guo, X., Ge, T., Oliver, M., and Li, L.: Faster carbon turnover in topsoil with straw addition is less beneficial to carbon sequestration than subsoil and mixed soil, Soil Science Society of America Journal, 86, 1431–1443, https://doi.org/10.1002/saj2.20412, 2022.

Duan, Y., Chen, L., Li, Y., Li, J., Zhang, C., Ma, D., Zhou, G., and Zhang, J.: Nitrogen input level modulates straw-derived organic carbon physical fractions accumulation by stimulating specific fungal groups during decomposition, Soil & Tillage Research, 225, https://doi.org/10.1016/j.still.2022.105560, 2023.

Even, R. J. and Cotrufo, F.: The ability of soils to aggregate, more than the state of aggregation, promotes protected soil organic matter formation, Geoderma, 442, 116760, https://doi.org/10.1016/j.geoderma.2023.116760, 2024.

Fang, Y., Singh, B., Cowie, A., Wang, W., Arachchi, M., Wang, H., and Tavakkoli, E.: Balancing nutrient stoichiometry facilitates the fate of wheat residue-carbon in physically defined soil organic matter fractions, Geoderma, 354, https://doi.org/10.1016/j.geoderma.2019.113883, 2019.

Ferreira, G., Oliveira, F., Soares, E., Schnecker, J., Silva, I., and Grandy, A.: Retaining eucalyptus harvest residues promotes different pathways for particulate and mineral-associated organic matter, Ecosphere, 12, https://doi.org/10.1002/ecs2.3439, 2021.

Fulton-Smith, S. and Cotrufo, M.: Pathways of soil organic matter formation from above and belowground inputs in a Sorghum bicolor bioenergy crop, Global Change Biology Bioenergy, 11, 971–987, https://doi.org/10.1111/gcbb.12598, 2019.

Haddix, M., Gregorich, E., Helgason, B., Janzen, H., Ellert, B., and Cotrufo, M.: Climate, carbon content, and soil texture control the independent formation and persistence of particulate and mineral-associated organic matter in soil, Geoderma, 363, https://doi.org/10.1016/j.geoderma.2019.114160, 2020.

Huys, R., Poirier, V., Bourget, M. Y., Roumet, C., Hattenschwiler, S., Fromin, N., Munson, A. D., and Freschet, G. T.: Plant litter chemistry controls coarse-textured soil carbon dynamics, Journal of Ecology, 110, 2911–2928, https://doi.org/10.1111/1365-2745.13997, 2022a.

Huys, R., Poirier, V., Bourget, M., Roumet, C., Hattenschwiler, S., Fromin, N., Munson, A., and Freschet, G.: Plant litter chemistry controls coarse-textured soil carbon dynamics, https://doi.org/10.5061/dryad.m63xsj45g, 2022b.

Kölbl, A., von Lutzow, M., and Kögel-Knabner, I.: Decomposition and distribution of N-15 labelled mustard litter (Sinapis alba) in physical soil fractions of a cropland with high- and low-yield field areas, Soil Biology and Biochemistry, 38, 3292–3302, https://doi.org/10.1016/j.soilbio.2006.04.010, 2006.

Kölbl, A., von Lutzow, M., Rumpel, C., Munch, J., and Kögel-Knabner, I.: Dynamics of C-13-labeled mustard litter (Sinapis alba) in particle-size and aggregate fractions in an agricultural cropland with high- and low-yield areas, Journal of Plant Nutrition and Soil Science, 170, 123–133, https://doi.org/10.1002/jpln.200625071, 2007.

Kou, X., Morien, E., Tian, Y., Zhang, X., Lu, C., Xie, H., Liang, W., Li, Q., and Liang, C.: Data for: Exogenous carbon turnover within the soil food web strengthens soil carbon sequestration through microbial necromass accumulation, https://doi.org/10.5061/dryad.mgqnk9949, 2023a.

Kou, X., Morrien, E., Tian, Y., Zhang, X., Lu, C., Xie, H., Liang, W., Li, Q., and Liang, C.: Exogenous carbon turnover within the soil food web strengthens soil carbon sequestration through microbial necromass accumulation, Global Change Biology, 29, 4069–4080, https://doi.org/10.1111/gcb.16749, 2023b.

Lavallee, J., Conant, R., Paul, E., and Cotrufo, M.: Incorporation of shoot versus root-derived 13C and 15N into mineral-associated organic matter fractions: results of a soil slurry incubation with dual-labelled plant material, Biogeochemistry, 137, 379–393, https://doi.org/10.1007/s10533-018-0428-z, 2018.

Leichty, S., Cotrufo, M., and Stewart, C.: Less efficient residue-derived soil organic carbon formation under no-till irrigated corn, Soil Science Society of America Journal, 84, 1928–1942, https://doi.org/10.1002/saj2.20136, 2021.

Lian, T., Wang, G., Yu, Z., Li, Y., Liu, X., and Jin, J.: Carbon input from C-13-labelled soybean residues in particulate organic carbon fractions in a Mollisol, Biology and Fertility of Soils, 52, 331–339, https://doi.org/10.1007/s00374-015-1080-6, 2016.

Liebmann, P., Wordell-Dietrich, P., Kalbitz, K., Mikutta, R., Kalks, F., Don, A., Woche, S., Dsilva, L., and Guggenberger, G.: Relevance of aboveground litter for soil organic matter formation - a soil profile perspective, Biogeosciences, 17, 3099–3113, https://doi.org/10.5194/bg-17-3099-2020, 2020.

Lyu, M., Homyak, P., Xie, J., Penuelas, J., Ryan, M., Xiong, X., Sardans, J., Lin, W., Wang, M., Chen, G., and Yang, Y.: Litter quality controls tradeoffs in soil carbon decomposition and replenishment in a subtropical forest, Journal of Ecology, https://doi.org/10.1111/1365-2745.14167, 2023.

Magid, J., Cadisch, G., and Giller, K.: Short and medium term plant litter decomposition in a tropical Ultisol elucidated by physical fractionation in a dual 13C and 14C isotope study, Soil Biology and Biochemistry, 34, 1273–1281, https://doi.org/10.1016/S0038-0717(02)00069-X, 2002.

Mitchell, E., Scheer, C., Rowlings, D., Conant, R., Cotrufo, M., and Grace, P.: Amount and incorporation of plant residue inputs modify residue stabilisation dynamics in soil organic matter fractions, Agriculture Ecosystems & Environment, 256, 82–91, https://doi.org/10.1016/j.agee.2017.12.006, 2018.

Neupane, A., Herndon, E., Whitman, T., Faiia, A., and Jagadamma, S.: Manganese effects on plant residue decomposition and carbon distribution in soil fractions depend on soil nitrogen availability, Soil Biology & Biochemistry, 178, https://doi.org/10.1016/j.soilbio.2023.108964, 2023.

Nunez, A., Cotrufo, F., and Schipanski, M.: Irrigation effects on the formation of soil organic matter from aboveground plant litter inputs in semiarid agricultural systems, Geoderma, 416, https://doi.org/10.1016/j.geoderma.2022.115804, 2022.

Nyamasoka-Magonziwa, B., Vanek, S., Ojiem, J., and Fonte, S.: Examining the contributions of maize shoots, roots, and manure to stable soil organic carbon pools in tropical smallholder farming soils, Geoderma, 425, https://doi.org/10.1016/j.geoderma.2022.116049, 2022.

Oliveira, R. S., Eller, C. B., Barros, F. de V., Hirota, M., Brum, M., and Bittencourt, P.: Linking plant hydraulics and the fast–slow continuum to understand resilience to drought in tropical ecosystems, New Phytologist, 230, 904–923, https://doi.org/10.1111/nph.17266, 2021.

Poeplau, C., Begill, N., Liang, Z., and Schiedung, M.: Root litter quality drives the dynamic of native mineral-associated organic carbon in a temperate agricultural soil, Plant and Soil, https://doi.org/10.1007/s11104-023-06127-y, 2023.

Pries, C., Bird, J., Castanha, C., Hatton, P., and Torn, M.: Long term decomposition: the influence of litter type and soil horizon on retention of plant carbon and nitrogen in soils, Biogeochemistry, 134, 5–16, https://doi.org/10.1007/s10533-017-0345-6, 2017.

Pries, C., Sulman, B., West, C., O'Neill, C., Poppleton, E., Porras, R., Castanha, C., Zhu, B., Wiedemeier, D., and Torn, M.: Root litter decomposition slows with soil depth, Soil Biology & Biochemistry, 125, 103–114, https://doi.org/10.1016/j.soilbio.2018.07.002, 2018.

Ridgeway, J., Morrissey, E., and Brzostek, E.: Plant litter traits control microbial decomposition and drive soil carbon stabilization, Soil Biology & Biochemistry, 175, https://doi.org/10.1016/j.soilbio.2022.108857, 2022.

Ridgeway, J., Kane, J., Starcher, H., Morrissey, E., and Brzostek, E.: BrzostekEcologyLab/InSitu_Incubation: Ridgeway et al., 2023 Data, https://doi.org/10.5281/zenodo.8408435, 2023a.

Ridgeway, J., Kane, J., Morrissey, E., Starcher, H., and Brzostek, E.: Roots selectively decompose litter to mine nitrogen and build new soil carbon, Ecology Letters, https://doi.org/10.1111/ele.14331, 2023b.

Schiedung, M., Bellè, S., Hoeschen, C., Schweizer, S., and Abiven, S.: Enhanced loss but limited mobility of pyrogenic and organic matter in continuous permafrost-affected forest soils, Soil Biology and Biochemistry, 178, https://doi.org/10.1016/j.soilbio.2023.108959, 2023.

Sokol, N., Kuebbing, S., Karlsen-Ayala, E., and Bradford, M.: Evidence for the primacy of living root inputs, not root or shoot litter, in forming soil organic carbon, New Phytologist, 221, 233–246, https://doi.org/10.1111/nph.15361, 2019.

Throckmorton, H., Bird, J., Monte, N., Doane, T., Firestone, M., and Horwath, W.: The soil matrix increases microbial C stabilization in temperate and tropical forest soils, Biogeochemistry, 122, 35–45, https://doi.org/10.1007/s10533-014-0027-6, 2015.

Wang, Y., Yu, Z., Li, Y., Wang, G., Liu, J., Liu, J., Liu, X., and Jin, J.: Microbial association with the dynamics of particulate organic carbon in response to the amendment of elevated CO2-derived wheat residue into a Mollisol, Science of the Total Environment, 607, 972–981, https://doi.org/10.1016/j.scitotenv.2017.07.087, 2017.

Xu, Y., Liu, K., Yao, S., Zhang, Y., Zhang, X., He, H., Feng, W., Ndzana, G., Chenu, C., Olk, D., Mao, J., and Zhang, B.: Formation efficiency of soil organic matter from plant litter is governed by clay mineral type more than plant litter quality, Geoderma, 412, https://doi.org/10.1016/j.geoderma.2022.115727, 2022.